iScience

CellPress
OPEN ACCESS

Article

Interfacial synthesis of large-area ultrathin polyimine nanofilms as molecular separation membrane

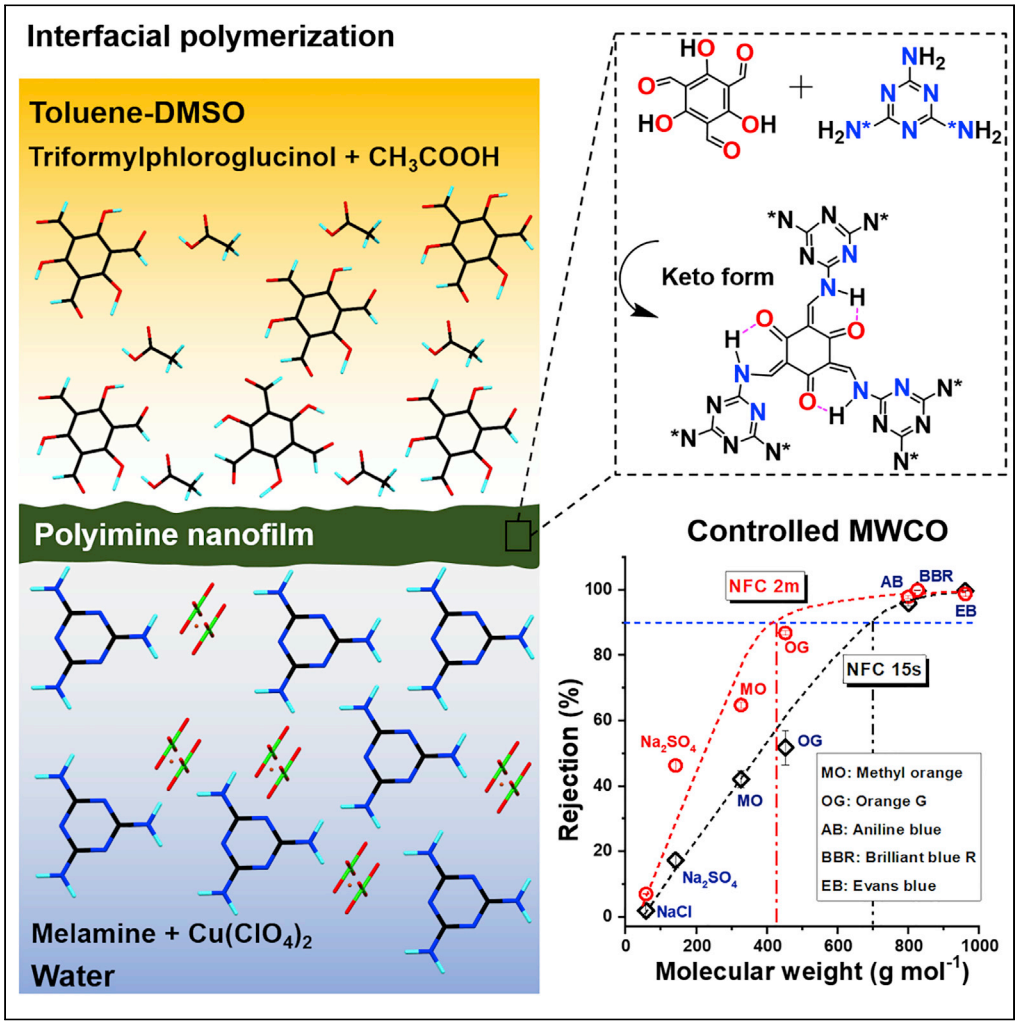

Karishma Tiwari, Solagna Modak, Pulak Sarkar, ..., Sumit Kumar Pramanik, Amitava Das, Santanu Karan

sumitpramanik@csmcri.res.in (S.K.P.)
amitava@iiserkol.ac.in (A.D.)
santanuk@csmcri.res.in (S.K.)

Highlights

Ultrathin porous polyimine nanofilms could be a close alternative to COF membranes

Large-area polyimine nanofilms are formed via interfacial polymerization

Transition metal ions favor the formation of the nanofilms at room temperature

Polyimine nanofilm membranes display superior permselectivity and tunable MWCO

Tiwari et al., iScience 25, 104027
April 15, 2022
https://doi.org/10.1016/j.isci.2022.104027

iScience

CellPress
OPEN ACCESS

Article

Interfacial synthesis of large-area ultrathin polyimine nanofilms as molecular separation membrane

Karishma Tiwari,[1,2,10] Solagna Modak,[3,8,10] Pulak Sarkar,[3,4] Santanu Ray,[5,9] Vasista Adupa,[6] K. Anki Reddy,[6] Sumit Kumar Pramanik,[1,4,*] Amitava Das,[1,7,*] and Santanu Karan[3,4,11,*]

SUMMARY

Thin film membranes of covalent organic frameworks are promising for high-permeance molecular separation. However, their synthesis needs a high temperature or longer reaction time, unsuitable for large-scale fabrication of thin film composite membranes. The ultrathin film of porous organic polymers as a separation layer of the composite membrane could be a close alternative to COF membranes. Here we report transition metal ion-catalyzed room temperature fabrication of the ultrathin (≈12 nm) polyimine nanofilms via interfacial polymerization of melamine and triformylphloroglucinol onto hydrolyzed polyacrylonitrile support within a short reaction time. Composite membranes exhibit high water permeance (≈78 L m^{-2} h^{-1} bar^{-1}), high rejection (99.6%) of brilliant blue R (825.9 g mol^{-1}), low rejection of NaCl (≈1.8%) and Na_2SO_4 (≈17%), and enable efficient molecular separation. The role of metal ion catalysts for large-area fabrication of the ultrathin polyimine nanofilm membranes used for molecular separation is demonstrated.

INTRODUCTION

Membrane technology has gained much attention as an alternative to conventional separation technologies because of their energy efficiency, scalability, and separation capability near the ambient temperature without any phase change (Marchetti et al., 2014). High-permeance nanofiltration membranes with controlled molecular weight cutoff (MWCO) promise selective separation of molecules based on their molecular weight (Sarkar et al., 2021a; You et al., 2021). However, high solute-solute selectivity is always imperative to achieve efficient molecular separation in nanofiltration (Sarkar et al., 2021b; Tiwari et al., 2020). For the last few decades, thin film composite and nanocomposite membranes with semi-aromatic or fully-aromatic polyamide separation layers have dominated the industry owing to their ease of fabrication for commercial production (Sarkar et al., 2020, 2021b; Karan et al., 2015; Gao et al., 2019). However, selective molecular separation from these membranes is not expected because of their tight network structure representing an MWCO of ≈300 g mol^{-1} and often show high rejection toward the monovalent and divalent ions (Sarkar et al., 2020, 2021b; Gao et al., 2019). Nanofiltration membranes with higher MWCO emphasizing dye salt separation applications have been developed to achieve negligible salt rejection (Jin et al., 2021; Liang et al., 2019; Zhang et al., 2020; Li at el., 2019). According to the convective flow model, fast water transport is achievable for nanofilm membranes as the permeance is inversely proportional to the thickness (Karan et al., 2012, 2015). Fast water transportation (permeance ≈53 L m^{-2} h^{-1} bar^{-1}) through erythritol-based polyester nanofiltration membrane for efficient dye/salt separation shows many such possibilities of developing efficient membranes with higher MWCO (Jin et al., 2021). Zwitterionic-functionalized MoS_2 nanosheet membranes (Liang et al., 2019), ultrathin trinity-coated membranes (Zhang et al., 2020), tannic acid-polyethyleneimine-crosslinked membranes (Li et al., 2019), and phytic acid-metal ion layer-by-layer-assembled (metal-organophosphate) membranes (You et al., 2019) are several examples of such composite membranes developed in recent years. Other than the polymeric membrane, efforts have been given to develop highly porous, chemically, and thermally stable covalent organic framework membranes with tunable pore sizes showing high selectivity and high permeance (Yuan et al., 2019). In addition, low density, high surface area, wide-range pore tuneability (~0.7–4.7 nm), and very high chemical/thermal stability (Yuan et al., 2011; El-Kaderi et al., 2007) make covalent organic frameworks (COFs) excellent materials for making separation membranes. Among different kinds of linkages (e.g.,

[1]Analytical and Environmental Science Division and Centralized Instrument Facility, CSIR-Central Salt and Marine Chemicals Research Institute, G. B. Marg, Bhavnagar, Gujarat 364002, India

[2]Department of Chemistry, School of Basic & Applied Sciences, Galgotias University, Greater Noida, Uttar Pradesh 203201, India

[3]Membrane Science and Separation Technology Division, CSIR-Central Salt and Marine Chemicals Research Institute, G.B. Marg, Bhavnagar, Gujarat 364002, India

[4]Academy of Scientific and Innovative Research (AcSIR), Ghaziabad, Uttar Pradesh 201002, India

[5]School of Environment and Technology, University of Brighton, Brighton BN2 4GJ, UK

[6]Department of Chemical Engineering, Indian Institute of Technology Guwahati, Assam 781039, India

[7]Department of Chemical Sciences and Centre for Advanced Functional Materials, Indian Institute of Science Education and Research Kolkata, Mohanpur, West Bengal 741246, India

[8]Present address: Hooghly Women's College, Pipulpati, Hooghly, West Bengal 712103, India

[9]Present address: Ceres Power Limited, Viking House, Foundry Lane, Horsham RH13 5PX, UK

[10]These authors contributed equally

[11]Lead contact

*Correspondence: sumitpramanik@csmcri.res.in (S.K.P.), amitava@iiserkol.ac.in (A.D.), santanuk@csmcri.res.in (S.K.)

https://doi.org/10.1016/j.isci.2022.104027

boron-oxygen, imine, etc.) present in COFs, imine-based COFs are less susceptible to hydrolysis and thus are employed in membrane technology (Dey et al., 2017; Kandambeth et al., 2017). However, large-scale production of COF-based thin film membranes is still a challenging issue because most COFs are prepared under a condition where a longer reaction time (typically a few days) or higher reaction temperature (>100°C) is required (Yuan et al., 2011; El-Kaderi et al., 2007; Dey et al., 2017; Kandambeth et al., 2017). With a proper selection of organic linkers and catalysts, COF-based thin film membranes were developed by changing reaction conditions. Wang et al. (2018) have prepared COFs@PSF composite membranes by reacting *p*-phenylenediamine with 1,3,5-triformylphloroglucinol at room temperature within a short reaction time (5–40 s) via the interfacial polymerization and postheating at 60°C for 5 min (Wang et al., 2018). By using this method, ~ 500 nm thick membrane was achieved with a relatively high water permeance of 50.0 L m^{-2} h^{-1} bar^{-1}. A two-dimensional imine-linked COF-LZU1 membrane with a thickness of ~400 nm was prepared on alumina tubes following *in situ* solvothermal synthesis (Fan et al., 2018). The membrane shows high water permeance (76 L m^{-2} h^{-1} bar^{-1}) with a preferential rejection of dyes larger than 1.2 nm (e.g., chrome black T), while allowing salts to permeate through (Fan et al., 2018). Similarly, 100–300 nm thick COF-LZU1@PES was developed by using interfacial polymerization of *p*-phenylenediamine with 1,3,5-triformylbenzene, enabling high water permeance of >80.0 L m^{-2} h^{-1} bar^{-1} and a preferential rejection of dyes larger than 1.5 nm (Su et al., 2021). To utilize thin films of COFs for large-scale membrane production, the film formation must be carried out at room temperature within a very short reaction time (e.g., ~2 min) to produce them in roll-to-roll. The short reaction time limits the formation of the crystalline structure of COFs in thin films as it produces an amorphous structure below a typical thickness of a few microns (Matsumoto et al., 2018). However, if crystallinity is compromised for the thin films, amorphous porous organic polymers (POPs) could be prepared in a shorter reaction time to define a trade-off between liquid permeance and crystallinity (or the thickness) in designing nanofilms with the desired MWCO (Tiwari et al., 2020). These prompted us to fabricate ultrathin membranes from amorphous POPs by using interfacial polymerization on a large area. In a typical synthesis, ~ 12 nm thick polyimine nanofilm was fabricated from the interfacial polymerization of melamine and triformylphloroglucinol (TFP) onto hydrolyzed polyacrylonitrile ultrafiltration support at room temperature in the presence of acetic acid and transition metal ion catalyst, $Cu(ClO_4)_2.6H_2O$, within a short reaction time of 15 s to 2 min. Composite membranes demonstrate the high water permeance (≈78 L m^{-2} h^{-1} bar^{-1}) with tunable MWCO between 425–700 g mol^{-1}. Observations on the nanofiltration studies under crossflow filtration with large permeate volume helped us to nullify the possibility of any physical adsorption of dye molecules (model solutes) on the membrane surface or within the support membrane as a plausible reason for the observed rejection of dye molecules.

RESULTS

Generally, acetic acid (Fan et al., 2018), scandium triflate (Matsumoto et al., 2017), and *p*-toluenesulfonic acid (Karak et al., 2017) are utilized to prepare polyimine networks through Schiff base condensation reaction. The catalytic role of transition metal ions (e.g., Cu^{2+}, Zn^{2+}, Pd^{2+}, etc.) for various organic reactions has been well explored in the literature (Anilkumar et al., 2020; Enthaler and Wu, 2015; Zhu et al., 2020). To the best of our knowledge, only a few reports are revealed where transition metal ions (Cu^{2+}) are used for Schiff base condensation reaction (Mobinikhaledi et al., 2009); however, interfacial preparation of polyimine nanofilms in the presence of Cu^{2+} ions is not reported yet. Catalyst-free bulk synthesis of the melamine-based microporous polymer (Schwab et al., 2009), and melamine-TFP-based COF (Bhadra et al., 2019) through Schiff base chemistry is well reported in the literature; however, it needs a higher temperature (120–180°C) and longer reaction time (72 h), a process that is unsuitable for the fabrication of thin film composite membranes. In this report, Cu^{2+} ions (perchlorate salt) are introduced for the interfacial fabrication of polyimine nanofilms, directly onto ultrafiltration supports within a very short reaction time (15 s) at room temperature. A polyimine nanofilm separation layer with thickness down to ≈12 nm was fabricated on top of the hydrolyzed polyacrylonitrile (HPAN) ultrafiltration support membranes by using interfacial polymerization of melamine (aqueous phase) and TFP (toluene-dimethylsulfoxide (DMSO)), where acetic acid in the toluene-DMSO phase and $Cu(ClO_4)_2.6H_2O$ in the aqueous phase were added as catalysts.

Figure 1A shows the proposed mechanism of formation of polyimine nanofilm by the Schiff base condensation of TFP and melamine in the presence of acetic acid and $Cu(ClO_4)_2.6H_2O$ catalyst. Details of the methodology adopted for the synthesis of TFP, the preparation of ultrafiltration polyacrylonitrile (PAN), and hydrolyzed PAN (HPAN) support membranes are provided in the Method Section. The ^{1}H and ^{13}C NMR spectra are presented in Figures S1 and S2, respectively. As reported in the literature, acetic acid catalyzes the reaction by protonation of carbonyl oxygen (Cordes and Jencks, 1962), while Cu^{2+} ion, a Lewis acid, is

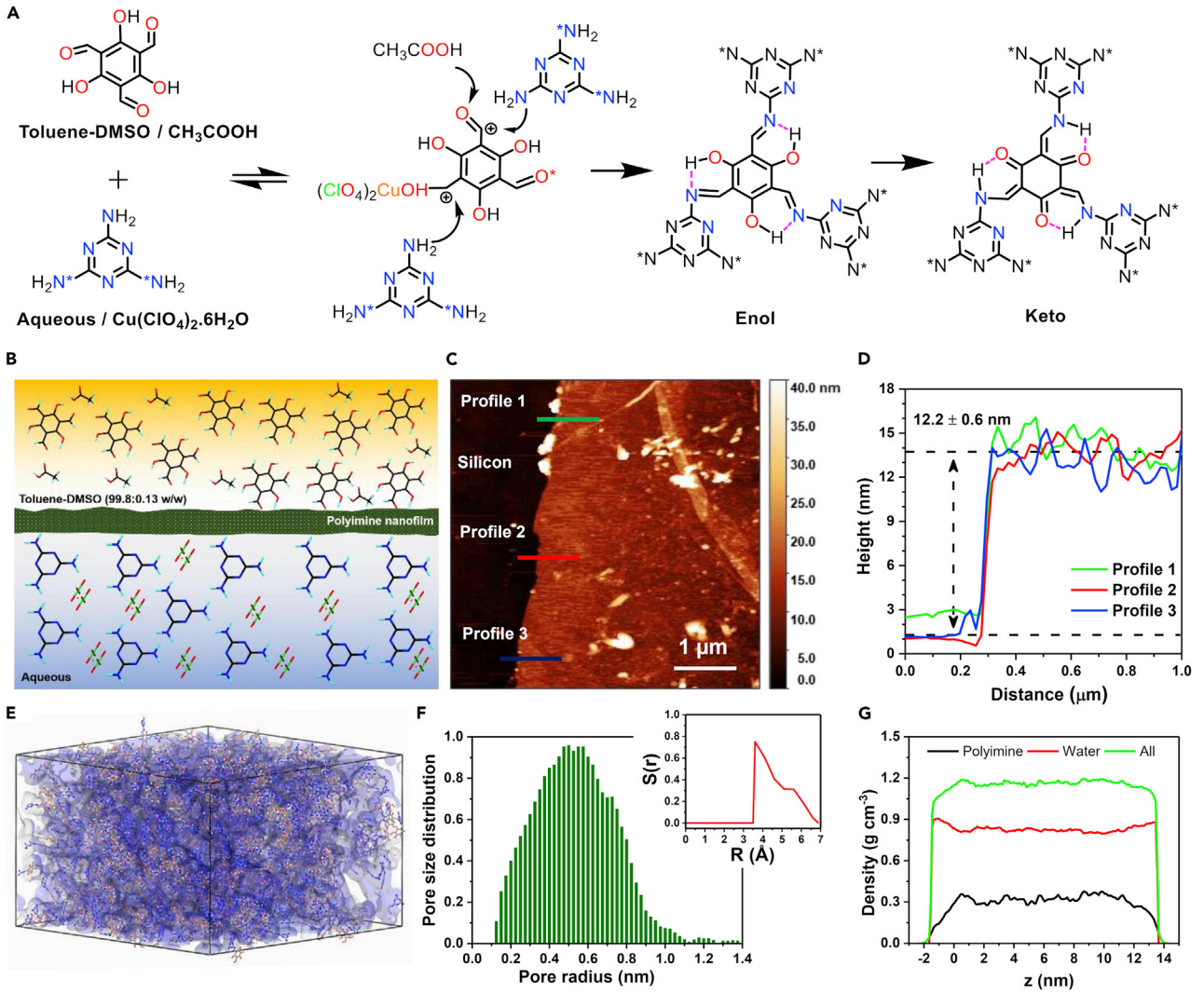

Figure 1. Synthesis of polyimine nanofilm via interfacial polymerization

(A) The proposed mechanism of the formation of polyimine in the presence of $Cu(ClO_4)_2.6H_2O$ and acetic acid (CH_3COOH) by the Schiff base condensation reaction of TFP and melamine.

(B) Schematic showing the formation of polyimine nanofilm via interfacial polymerization of toluene-DMSO solution of TFP and acetic acid (an organic phase) with melamine and $Cu(ClO_4)_2.6H_2O$ (an aqueous phase).

(C and D) AFM cross-sectional image and AFM height profile of a freestanding polyimine nanofilm formed at the liquid-liquid interface (reaction time: 2m) and transferred onto a silicon wafer. Freestanding nanofilm was prepared from the interfacial polymerization reaction of toluene-DMSO (0.13 wt%) solution of TFP (0.023 wt%) with an aqueous solution of melamine (0.1 wt%) in the presence of acetic acid (0.061 wt%) and $Cu(ClO_4)_2.6H_2O$ (0.02 wt%).

(E) Three-dimensional view of an amorphous polyamide cell containing a network structure of the polymer. Blue color represents the accessible surface at a probe radius of 2.0 Å.

(F and G) The pore size distribution and (G) the density profile of the nanofilm derived from the simulation experiment.

also presumed to bind to carbonyl oxygen to facilitate the polymerization reaction (Figures S3 and S4). Because of the presence of intramolecular O-H···N type hydrogen bonding, the prepared polyimine network undergoes keto-enol tautomerization and predominantly exists in a more stable keto state (Figure 1A) (Kandambeth et al., 2012). Figure 1B shows the schematic presentation of the formation of polyimine nanofilm by using interfacial polymerization, where the aqueous phase containing melamine (0.1 wt %) and catalyst $Cu(ClO_4)_2.6H_2O$ (0.02 wt%) were soaked in HPAN ultrafiltration support and reacted with TFP organic phase containing 0.023 wt% of TFP and 0.061 wt% acetic acid in the toluene-DMSO (99.81:0.13 w/w). Suspension of TFP (0.023 wt%) in a very small amount of DMSO (0.13 wt%) and acetic acid (0.061 wt %) before addition to toluene (99.81 wt%) enhances the solubility of TFP in toluene. Polyimine

nanofilm composite membranes were fabricated with varying interfacial polymerization times at 15 s (NFCM 15s Cu(II)) and 2 min (NFCM 2m Cu(II)), respectively. Because of the structural instability of the polyimine nanofilms in dimethylformamide, polyimine nanofilms could not be isolated from the composite membrane, which is frequently used to isolate the nanofilms from support for their characterization in the form of a freestanding film (Sarkar et al., 2020, 2021b). Thus, to measure the thickness of the nanofilm, an identical freestanding polyimine nanofilm was prepared at the bulk aqueous-organic interface in a glass Petri dish and transferred onto different supports (e.g., silicon wafer, gold-coated silicon wafer, and porous anodic alumina). The thickness of the nanofilm formed on the HPAN support was similar to the nanofilm formed at the aqueous-organic bulk interface (see later – the cross-sectional SEM and TEM image). The aqueous phase containing melamine (0.1 wt%) and catalyst $Cu(ClO_4)_2.6H_2O$ (0.02 wt%) was reacted with TFP (0.023 wt%) in the presence of acetic acid (0.061 wt%) in toluene-DMSO (99.81:0.13 w/w) solution to form a freestanding nanofilm by using interfacial polymerization for 2 min (FSNF 2m Cu(II); polymerization time: 2 min). Atomic force microscopy (AFM) image and the height profile of a section of freestanding polyimine nanofilm, FSNF 2m Cu(II), transferred onto a silicon wafer, show a thickness of ~12.2 nm (Figures 1C and 1D). A smooth surface morphology with occasional folding was identified, which was inherent to the process followed for transferring nanofilm on the silicon wafer (Karan et al., 2015). The AFM image confirms that a continuous defect-free polyimine nanofilm could be produced from melamine and TFP by using interfacial polymerization in a very short polymerization time. The observed molecular separation performance also supports the formation of a defect-free nanofilm. The porous structure of the polyimine nanofilm was visualized by simulating the polymer structure. Figure 1E shows a three-dimensional view of an amorphous polyimine cell containing a network structure of polyimine with an equivalent thickness of the nanofilm produced by using interfacial polymerization. The molecular dynamics study was carried out to know the structure of the polyimine nanofilm at the molecular level. All the force field parameters for monomers and the polymer were obtained from CHARMM General Force Field (CGenFF) (Vanommeslaeghe et al., 2010, 2012b; Yu et al., 2012; Vanommeslaeghe and MacKerell, 2012a) interface version 1.0.0 and the force field version 3.0.1 (Figures S5–S7). All the simulations were carried out on NAMD (Philips et al., 2020). A wide distribution of pores with a radius peaked around of 0.5 nm was found in the nanofilm (Figure 1F). The structural features of the polyimine are represented in terms of the order parameter ($S(r)$) (Wei et al., 2016; Sarkar et al., 2021c).

$$S(r) = \left[\frac{3cos^2(\theta(r)) - 1}{2}\right] \quad \text{(Equation 1)}$$

where $\theta(r)$ is the angle between the planes of melamine and the TFP at a radial distance r (Wei et al., 2016; Sarkar et al., 2021c). $S=1$ corresponds to a fully ordered packing, and $S=0$ represents a completely random structure (Wei et al., 2016; Sarkar et al., 2021c). The structural parameter $S(r)$ as a function of r is presented in the inset of Figure 1F. A peak corresponding to the ordered packing is observed at a distance of 3.5 Å, referred to as the interplanar arrangement between the melamine and TFP units (Wei et al., 2016; Sarkar et al., 2021c). These interactions drop sharply with increasing distance and represent a small plateau at ~ 5 Å, corresponding to the existence of T-shaped stacking between the melamine and TFP units (Wei et al., 2016; Sarkar et al., 2021c). The calculated density profiles of the nanofilm, water, and the overall system across the thickness are presented in Figure 1G. A low density of ~0.35 g cm^{-3} of the nanofilm represents a high overall porosity.

We conducted many interfacial polymerization reactions between melamine and TFP to produce polyimine nanofilms without catalyst $Cu(ClO_4)_2.6H_2O$ in the aqueous phase. In one case, the scanning electron microscopy (SEM) image (Figure 2A) supported the formation of a smooth and defect-free nanofilm; however, the molecular separation performance of the nanofilm composite membrane made on HPAN support conducted under crossflow filtration conditions was insignificant as the rejection of brilliant blue R (BBR; molecular weight = 825.9 g mol^{-1}) was limited to 93.4% (Table S1) with extremely high pure water permeance of 270 L m^{-2} h^{-1} bar^{-1}. We identified this rejection as an adsorption phenomenon of BBR on the membrane surface and within the support membrane, not the true rejection by the polyimine nanofilm separation layer. It is worth mentioning that the HPAN supports are widely used for making nanofiltration membranes. Our recent articles (Sarkar et al., 2021b, 2021c) present the superiority of the HPAN support in terms of the high water permeance of the final composite membranes. Compared to the PAN support, more than twice that of the water permeance was achieved for the nanofilms prepared on HPAN support (Sarkar et al., 2021b, 2021c). The hydrophilicity of the support membrane plays a significant role in achieving the stoichiometric equilibrium condition of the amine monomer at the interface during the interfacial polymerization

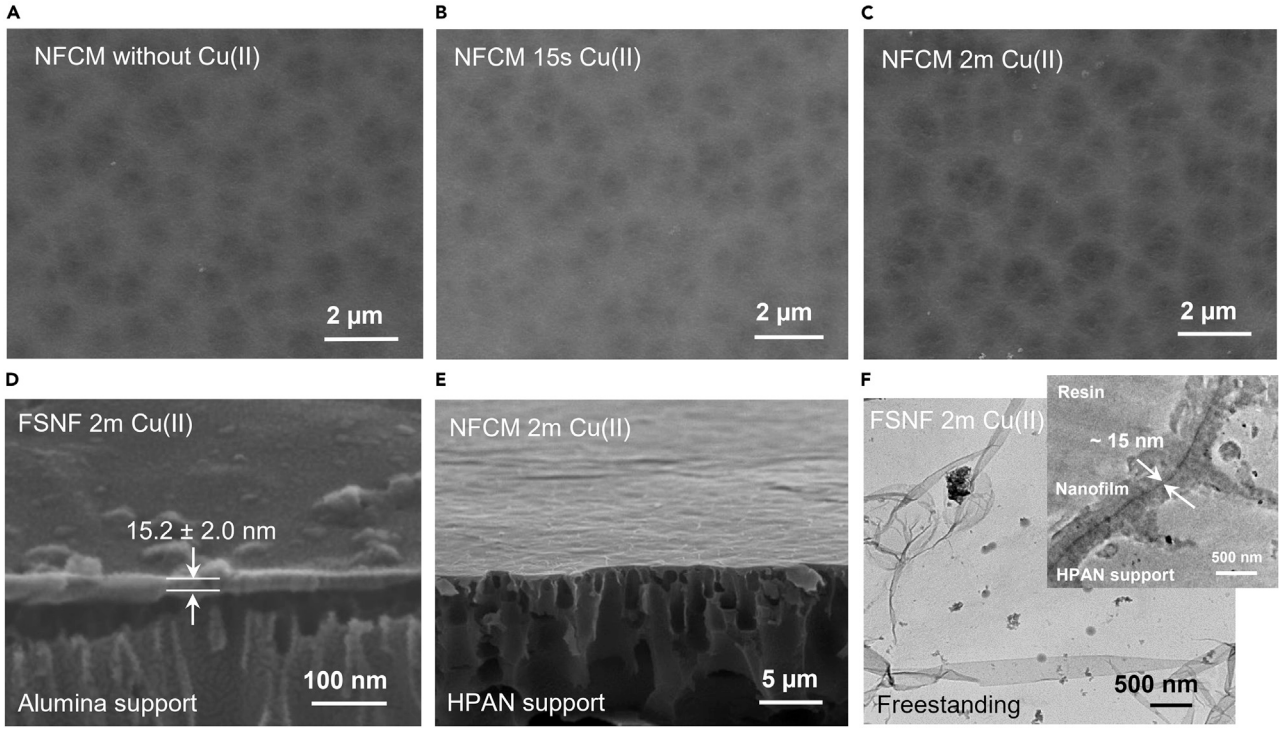

Figure 2. Surface morphology of the nanofilm and their composite membrane

(A) SEM images of polyimine nanofilm composite membrane prepared via interfacial polymerization of melamine aqueous phase (without the addition of $Cu(ClO_4)_2$ in the aqueous phase) and the toluene-DMSO solution of TFP in the presence of acetic acid (CH_3COOH) onto HPAN support (reaction time 1 min). (B and C) represent SEM images of polyimine nanofilm composite membranes prepared on HPAN support. NFCM 15s Cu(II) and NFCM 2m Cu(II) were prepared in the presence of $Cu(ClO_4)_2.6H_2O$ and acetic acid (CH_3COOH) under identical experimental conditions by maintaining the polymerization reaction time at 15s and 2m, respectively.

(D) Cross-sectional SEM image of a freestanding polyimine nanofilm, FSNF 2m Cu(II), transferred onto alumina support.

(E) Cross-sectional SEM image of a polyimine nanofilm composite membrane, NFCM 2m Cu(II) prepared onto HPAN support.

(F) TEM images of freestanding polyimine nanofilm, FSNF 2m Cu(II), transferred onto a TEM copper grid. Inset shows the cross-sectional TEM image of NFCM 2m Cu(II) membrane fabricated on HPAN.

(Sarkar et al., 2021b, 2021c). The presence of –COOH group on HPAN support makes it more hydrophilic than PAN with much higher water permeance.

In the presence of $Cu(ClO_4)_2.6H_2O$ in the aqueous phase, the nanofilms were fabricated under 15 s and 2 min reaction times (Figures 2B and 2C). These nanofilms also showed a smooth surface morphology, as observed in Figure 2A. The cross-sectional SEM image of the freestanding nanofilm fabricated at the bulk organic-aqueous interface, FSNF 2m Cu(II) (reaction time: 2 min), and transferred onto porous anodic alumina support reveals a thickness of 15.2 $\pm$ 2.0 nm (Figure 2D). This is in close agreement with the nanofilm thickness measured by using the AFM height profile (Figure 1D). Relatively higher thickness could be because of the thickness of the gold coating employed for SEM imaging. The cross-sectional SEM image of the nanofilm composite membrane fabricated on HPAN support, NFCM 2m Cu(II), reveals a very thin polyimine layer on the support (Figure 2E); however, the thickness measurement from such an image was not possible because of the indifferent contrast of the support and the nanofilm. The transmission electron microscopy (TEM) image of a freestanding nanofilm FSNF 2m Cu(II) produced at the bulk organic-aqueous interface and transferred onto a TEM grid shows the continuous and defect-free characteristics (Figure 2F). We have conducted the TEM cross-sectional imaging of NFCM 2m Cu(II) fabricated on HPAN support, which measures a thickness of the nanofilm (inset of Figure 2F) $\sim$ 15 nm. Thus, the thickness of the polyimine nanofilm formed at the bulk organic-aqueous interface and on the HPAN support is similar to each other.

Fourier transformed infrared spectra (FTIR) spectrum of melamine, shown in Figure 3A, represents the characteristic absorption bands at 3130–3470 cm^{-1} for $-NH_2$ stretching. The absorption band at 3340 cm^{-1} and

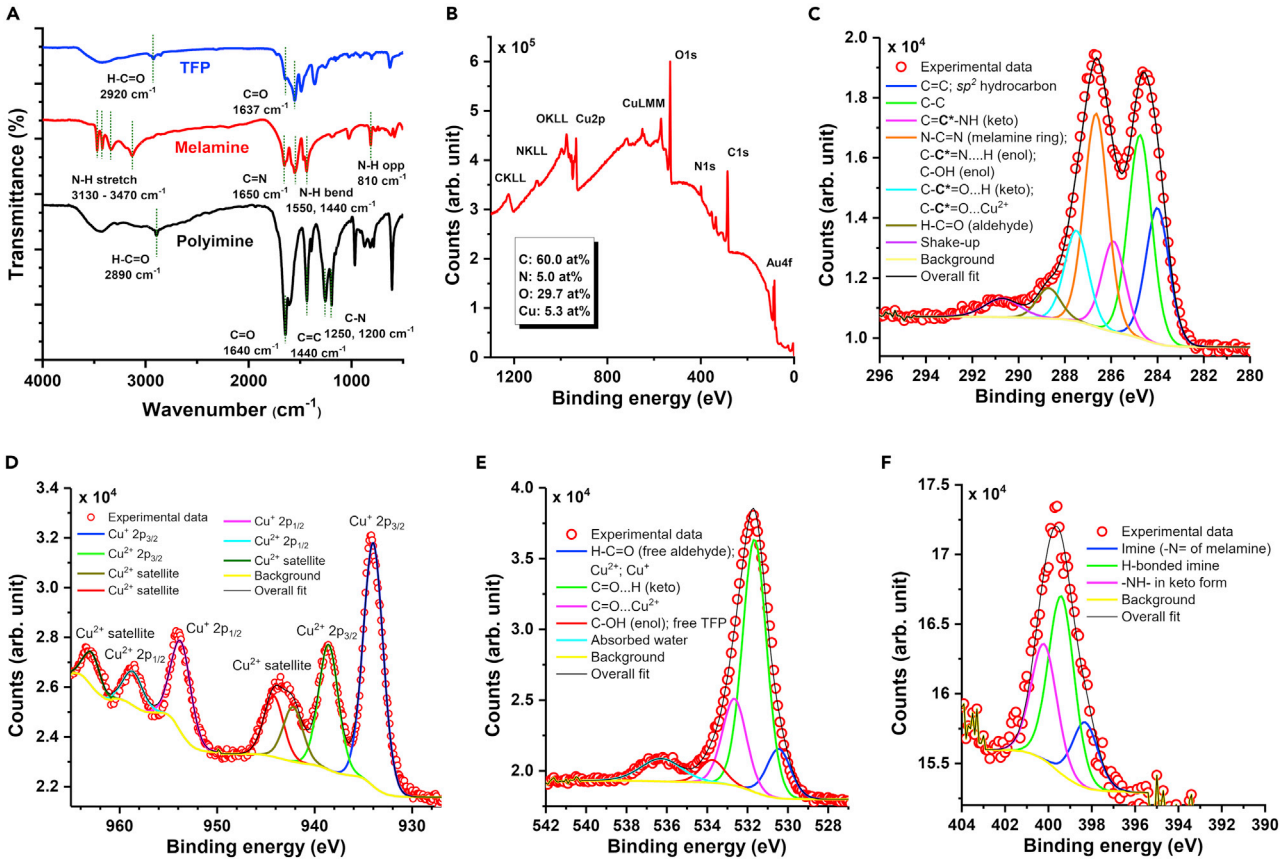

Figure 3. Characterization of the freestanding nanofilm using FTIR and XPS

(A) FTIR spectra of TFP, melamine and the freestanding nanofilm (FSNF 2m Cu(II)).

(B–F) XPS results of the nanofilm. (B) XPS survey spectrum, (C) XPS C1s, (D) XPS Cu2p, (E) XPS O1s, and (F) XPS N1S core-level spectra of the freestanding nanofilm (FSNF 2m Cu(II)) transferred on Au coated silicon wafer. Freestanding nanofilm was prepared from the interfacial polymerization reaction of toluene-DMSO (0.13 wt%) solution of TFP (0.023 wt%) with an aqueous solution of melamine (0.1 wt%) in the presence of acetic acid (0.061 wt%) and $Cu(ClO_4)_2.6H_2O$ (0.02 wt%) for a reaction time of 2 min.

3130 cm^{-1} are originated from asymmetrical and symmetrical stretching vibrations of the $–NH_2$ group. The characteristic absorption bands of TFP for –OH, -(H)CO and >C=O are observed at 3425 cm^{-1}, 2920–2845 cm^{-1}, and at 1637 cm^{-1}, respectively. The absorption band observed at 1640 cm^{-1} in FTIR spectra of polyimine is assigned for the carbonyl group, and a sharp peak at 1440 cm^{-1} is attributed to the C=C stretching of the keto group. The absorption band at 1200–1250 cm^{-1} could have originated from the -C-N stretching vibrations. The structural analysis of the freestanding polyimine nanofilm, FSNF 2m Cu(II), transferred onto the gold-coated silicon wafer was performed with X-ray photoelectron spectroscopy (XPS). The XPS survey spectrum of the nanofilm is presented in Figure 3B, where the existence of the constituent elements of polyimine is evident. The elemental composition was C = 60.0 at%, N = 5.0 at%, O = 29.7 at%, and Cu = 5.3 at%. The presence of Cu is because of the binding of Cu^{2+} within the polyimine network with highly electronegative nitrogen and oxygen atoms (Figure S8). The core-level C1s, Cu2p, and O1s spectra of the nanofilms were analyzed to further understand the chemical crosslinking of the nanofilms (Figures 3C–3E). The deconvoluted results from the C1s spectrum show a contribution of the C=C-NH (keto) of 11.4 at%, N-C=N (melamine ring)/C-C=N ….H (enol)/C-OH (enol) of 26.9 at%, C-C=O … H (keto)/C-C=O … Cu^{2+} of 11.4 at%, and a small amount of unreacted aldehyde (H-C=O) group of 3.8 at%. This confirms the presence of both the enol and keto forms of polyimine. However, the predominant form could be the keto form, as prescribed by others (Kandambeth et al., 2012). The deconvoluted results from the Cu2p spectrum support the presence of Cu^{+} and Cu^{2+} linked to the polyimine network. However, the formation of CuO and Cu_2O is most likely because the nanofilm was exposed to air, and it is difficult to confirm their presence from the Cu2p core-level XPS spectrum. The C=O … H of the keto form was confirmed from the O1s spectrum (Figure 3E) and is the most dominant (~56 at%) in the

Table 1. Water permeance and rejection performance of polyimine nanofilm composite membranes with different salts and dye molecules as feed

		Nanofiltration performance of the polyimine nanofilm composite membranes							
Membranes	Feed	PWP (LMH bar)	NaCl (58.4 g mol^{-1})	Na_2SO_4 (142.0 g mol^{-1})	Methyl orange (327.3 g mol^{-1})	Orange G (452.4 g mol^{-1})	Aniline blue (799.8 g mol^{-1})	Brilliant blue R (825.9 g mol^{-1})	Evans blue (960.8 g mol^{-1})
NFCM 15s Cu(II) (at 2 bar)	Permeance (L m^{-2} h^{-1} bar^{-1})	78.4 ± 3.7	67.6 ± 4.8	51.2 ± 4.9	50.9 ± 1.9	73.9 ± 5.5	56.5 ± 2.2	70.8 ± 4.8	63.7 ± 4.1
	Rejection (%)	–	1.8 ± 2.1	17.2 ± 2.2	42.0 ± 2.5	51.7 ± 5.3	95.9 ± 0.8	99.7 ± 0.02	99.6 ± 0.1
NFCM 2m Cu(II) (at 2 bar)	Permeance (L m^{-2} h^{-1} bar^{-1})	49.7 ± 3.2	42.2 ± 1.0	26.7 ± 1.7	42.2 ± 0.5	49.9 ± 1.5	39.5 ± 0.7	46.7 ± 2.1	43.4 ± 1.7
	Rejection (%)	–	6.9 ± 0.1	46.2 ± 1.7	64.7 ± 0.8	86.8 ± 0.7	97.8 ± 0.4	99.9 ± 0.03	98.7 ± 0.8
NFCM 2m Cu(II) (at 5 bar)	Permeance (L m^{-2} h^{-1} bar^{-1})	28.9 ± 2.6	21.7 ± 0.5	18.3 ± 1.9	26.3 ± 1.8	26.1 ± 1.5	23.3 ± 0.5	21.4 ± 0.2	27.9 ± 0.1
	Rejection (%)	–	10.4 ± 3.8	65.7 ± 12.8	66.6 ± 10.8	86.9 ± 5.0	98.7 ± 0.1	99.9 ± 0.01	99.7 ± 0.1

NFCM 15s Cu(II): Organic phase: TFP 0.023 wt% + AcOH 0.061 wt%; Aqueous phase: MEL 0.1 wt% + $Cu(ClO4)_2.6H_2O$ 0.02 wt% IP time: 15 s; Post-heating: 70°C for 3 min. NFCM 2m Cu(II): Organic phase: TFP 0.023 wt% + AcOH 0.061 wt%; Aqueous phase: MEL 0.1 wt% + $Cu(ClO4)_2.6H_2O$ 0.02 wt% IP time: 2 min; Post-heating: 70°C for 3 min. PWP: Pure water permeance (LMHbar = L m^{-2} h^{-1} bar^{-1}).

polyimine. Thus the FTIR result indicates that the –OH group of the TFP undergo keto-enol tautomerization to form a more stable keto moiety. Moreover, the presence of stretching bands at 3430 cm^{-1} and 2890 cm^{-1} for $–NH_2$/-OH and –CHO groups, respectively, in the FTIR spectra of polyimine indicates the existence of unreacted aldehyde groups of TFP (also supported by the O1s XPS results). The deconvoluted N1s spectra in Figure 3F reveals the presence of imine moiety (-*N* =) of melamine amine ring (18.2 at%), the imine hydrogen-bonded with $-NH_2$ of melamine and -OH group of unreacted TFP (49.5 at%), and the amine (-NH-) in the keto form (32.3 at%). The surface zeta potential measurement of the polyimine nanofilms indicates the negatively charged surface ($\xi = -18$ to -25 mV) of the composite membrane at pH 7 (Figure S9). These results also support the presence of the unreacted aldehyde group of TFP on the surface of the nanofilm and thus the nanofilm could be poorly crosslinked from the top.

In the presence of $Cu(ClO_4)_2.6H_2O$, we successfully achieved the formation of polyimine nanofilm composite membranes on HPAN support. Membranes were employed for nanofiltration and molecular separation applications in the aqueous feed under crossflow conditions at 2 bar or 5 bar (Table 1). To find the best interfacial polymerization conditions, the nanofiltration experiment was conducted using several composite membranes prepared under optimum conditions, as listed in Tables 1 and S1. Nanofilm composite membrane prepared in the absence of $Cu(ClO_4)_2.6H_2O$ showed a very high water permeance of 270 ± 93 L m^{-2} h^{-1} bar^{-1} and 93.4% rejection of BBR dye. Visual observation after the filtration test confirms the immense absorption of dye within the membrane (Figure S10). This also confirms the formation of a defective polyimine layer, and the observed rejection was attributed to the absorption of dye within the composite structure. Further, different nanofilm composite membranes were prepared in the presence of $Cu(ClO_4)_2.6H_2O$ by varying the polymerization reaction time and posttreatment with methanol, dimethylacetamide, NaOH (pH = 7.4 and 10), and room humidity (87%) (Table S1). The permeability of the polyimine composite membrane, NFCM 15s Cu(II), was investigated in pure solvents (e.g., water, methanol, acetonitrile, and isopropanol) (Figure S11). NFCM 15s Cu(II) membrane exhibited a very high pure water permeance (PWP) of 78.4 L m^{-2} h^{-1} bar^{-1}. The permeability was decreased in the organic solvents, methanol (26.4 L m^{-2} h^{-1} bar^{-1}), acetonitrile (56.7 L m^{-2} h^{-1} bar^{-1}), and isopropanol (1.7 L m^{-2} h^{-1} bar^{-1}). The high water permeance may be because of the strong interaction of water and the polar groups (-OH or C=N) of polyimine nanofilm, whereas the decreased permeance in methanol and acetonitrile may be because of the swelling-driven compaction of the loosely packed microstructure of the polyimine nanofilm in these solvents. Please note that the polyimine nanofilm is highly porous with a very low density of ~0.35 g cm^{-3} (Figure 1G) and thus the structural change in the organic solvents is most likely to occur. The PWP was decreased as the polymerization reaction time was increased from 15 s to 2 min, owing to the formation of a tight network structure (Table 1). The high pure water permeance and water stability of the membranes allowed us to further investigate the rejection efficiency of various salts and dyes in the aqueous solution (Table 1). A high BBR rejection value of >99% and a very low rejection of NaCl <15% were observed for

all the membranes when tested under different applied pressures (Tables 1 and S1). Physical compaction of the nanofilm composite membrane, NFCM 2m Cu(II), was also observed when tested at high pressure (5 bar) and showed a decrease in pure water permeance to a value of 28.9 L m^{-2} h^{-1} bar^{-1} while maintaining a high rejection of BBR 99.9% (Table 1).

The nanofiltration performance of the composite membrane, NFCM 15s Cu(II) tested for different salts (NaCl & Na_2SO_4), negatively charged dye molecules, e.g., methyl orange (MO), orange G (OG), aniline blue (AB), Evans blue (EB), and brilliant blue R (BBR) and positively charged dye, rhodamine B (RhB) showed high water permeance (Figure 4A) and very high rejection of BBR (99.7%), Evans blue (EB, 99.6%), aniline blue (95.9%), moderate rejection of orange G (51.7%), and MO (42.0%), and low rejection of NaCl (1.8%), Na_2SO_4 (17.2%) and rhodamine B (17.5%) (Figure 4B). The negatively charged molecules were preferentially rejected by the nanofilm composite membranes owing to their negatively charged surface, where the Donnan exclusion-based separation is favorable. When the polymerization time was increased to 2 min, nanofilm composite membrane, NFCM 2m Cu(II) showed a decrease in pure water permeance (49.7 L m^{-2} h^{-1} bar^{-1}) and an increase in rejection of salts and dye molecules (Figure S12). UV-visible absorption spectra and the photograph of permeate and feed aqueous solutions of BBR and MO dye are shown in Figure 4C. To evaluate the separation ability of the composite membrane in the mixed feed, a mixed feed solution of BBR and NaCl was also conducted. Selective separation of NaCl ($R < 1\%$) from the mixed feed with a very high rejection of BBR ($R = 99.8\%$) (Table S2) was achieved. A mixed feed solution of Na_2SO_4 and BBR showed an increased rejection of Na_2SO_4 ($R = 38.3\%$), while a very high rejection of the BBR ($R = 99.7\%$) was also mentioned (Table S2). Selective separation of a small molecule was also achieved for a mixed feed of a larger dye BBR (MW = 825.9 g mol^{-1}) and a smaller dye MO (MW = 327.3 g mol^{-1}). UV-visible absorption spectra showed a similar rejection of MO (39.4%) as it was for the pure MO feed and high rejection of BBR (98.9%), demonstrating the possibility of separation of the anionic dye mixture according to their difference in molecular weight (Figure 4D).

Molecular structures of different dye molecules are provided in Table S3. The rejection of different dye molecules depends on their molecular weight. The MWCO for polyimine nanofilm composite membranes was determined from the plot of rejection of salts and negatively charged solutes with their molecular weights. NFCM 2m Cu(II) showed moderate MWCO of 425 g mol^{-1}, whereas NFCM 15s Cu(II) showed a higher MWCO of 700 g mol^{-1} (Figure 4E). The presence of the porous structure of the polyimine nanofilms was further confirmed from the linear relationship between the liquid permeance and the inverse of viscosity of the liquid feed chosen from water, water-methanol mixture, and isopropanol (Figure 4F). A small deviation from the linear relationship was observed in the methanol-water mixture because of the microstructural changes of the polyimine nanofilm in presence of a very small amount of methanol in the mixture (Figure 4F). In addition, this linear relationship was also maintained for pure methanol and acetonitrile (Figure S11); however, the permeance of both the solvents was much lower compared to the pure water permeance and the expected convective flow model.

DISCUSSION

In summary, we have utilized acetic acid and transition metal ions, $Cu(ClO_4)_2.6H_2O$, for large-area fabrication of polyimine based porous organic polymers (POPs) on HPAN UF support. The polyimine nanofilms prepared via interfacial polymerization of TFP and melamine were utilized as a nanofiltration membrane for molecular separation in the aqueous feed. A nanofilm composite membrane with a thickness of 12.2 nm showed high water permeance of ~78 L m^{-2} h^{-1} bar^{-1}, high rejection of BBR dye (99.6%), and low rejection of monovalent/divalent ions (<20%). The interfacial synthesis of ultrathin imine-based porous polymers can be adopted for the roll-to-roll production of composite membranes, which may pave the way to address the unmet challenges for the treatment of wastewater, including feed water of molecular dye, mono/divalent salt, and their mixture, with high water permeance and low salt rejection.

Limitations of the study

The ultra-permeable membranes have a general limitation on the pressure drop across the porous support where the selective layer of the composite membranes sits. A proper choice of support may even lead to much higher liquid permeance without compromising the separation property (Karan et al., 2015). Further development and study on the formation of the polyimine nanofilms on highly porous ultrafiltration support are needed to achieve superior membranes for molecular separation.

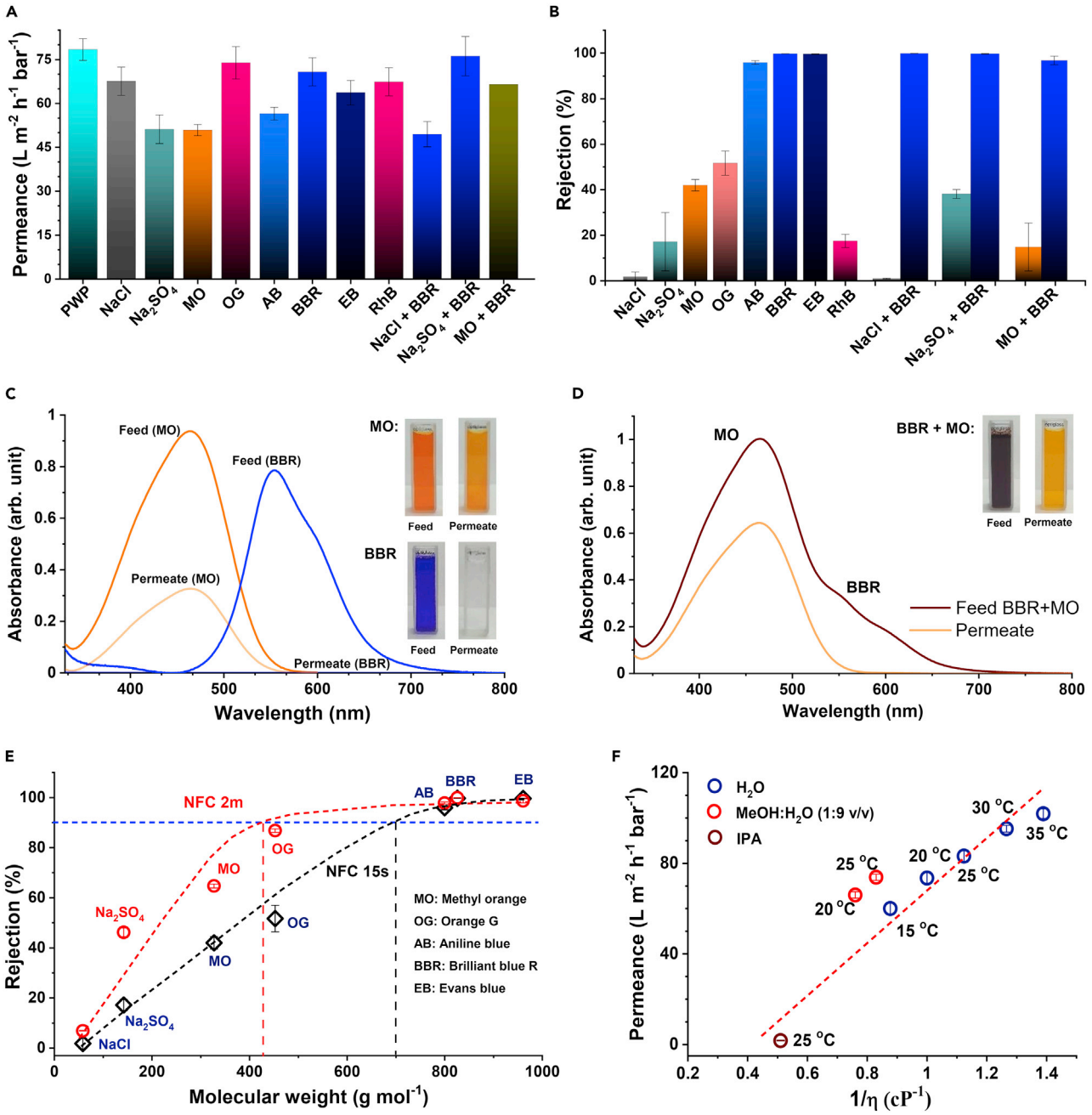

Figure 4. Nanofiltration performance of polyimine nanofilm composite membranes under crossflow condition at 2 bar

(A) Water permeance and (B) rejection of the composite membrane, NFCM 15s Cu(II), for different salts, dye molecules, and mixed feed solutions in water, respectively.

(C and D) UV-visible absorption spectra of the feed and permeate solution. (C) UV-visible absorption spectra of BBR and MO, (D) UV-visible spectra of a mixture of BBR and MO in the aqueous feed and permeate for NFCM 2m Cu(II). Insets show the photograph of the feed and permeate solutions taken in a cuvette.

(E) MWCO was obtained for composite membranes NFCM 15s Cu(II) and NFCM 2m Cu(II), from the plot of rejection versus the molecular weight of solutes.

(F) The plot of solvent permeance against their viscosity for the polyimine nanofilm composite membrane, NFCM 15s Cu(II).

STAR★METHODS

Detailed methods are provided in the online version of this paper and include the following:

- KEY RESOURCES TABLE
- RESOURCE AVAILABILITY

SUPPLEMENTAL INFORMATION

Supplemental information can be found online at https://doi.org/10.1016/j.isci.2022.104027.

ACKNOWLEDGMENTS

S.K. acknowledges the financial support from the Science and Engineering Research Board, Department of Science and Technology, Government of India (project grant number EMR/2017/000251 and SB/S2/RJN-030/2016). A.D. acknowledges the financial support from the Science and Engineering Research Board, Department of Science and Technology, Government of India (project grant number JCB/2017/000004). K.T. acknowledges the CSIR, New Delhi, for providing CSIR-RA fellowship. S.R. acknowledges the funding received under the Global Challenge Research Fund (GCRF) Business Case through the University of Brighton, UK. K.T., S.M., P.S., S.K.P., and S.K. acknowledge the technical support from the Centralized Instrumental Facility, CSIR-CSMCRI, Bhavnagar. A PRIS number (CSIR-CSMCRI – 61/2021) has been assigned for this manuscript.

AUTHOR CONTRIBUTIONS

S.K., S.K.P., and A.D. supervised the project. K.T. synthesized the monomer. K.T. and S.M. fabricated the membranes, carried out the experimental work, and analyzed the data. P.S. carried out the cross-sectional TEM and streaming potential study. S.R. carried out the XPS study. V.A. and K.A.R. carried out the computational work. K.T. and S.K. wrote the manuscript. S.K. conceptualized the project. A.D. and S.K. contributed to the fund acquisition.

DECLARATION OF INTERESTS

The authors declare no competing interests.

Received: November 4, 2021
Revised: February 16, 2022
Accepted: March 1, 2022
Published: April 15, 2022

REFERENCES

Anilkumar, G., and Saranya, S. (2020). Copper Catalysis in Organic Synthesis (Wiley-VCH Verlag GmbH & Co. KGaA).

Bhadra, M., Kandambeth, S., Sahoo, M.K., Addicoat, M., Balaraman, E., and Banerjee, R. (2019). Triazine functionalized porous covalent organic framework for photo-organocatalytic e−z isomerization of olefins. J. Am. Chem. Soc. *141*, 6152–6156.

Cordes, E.H., and Jencks, W.P. (1962). On the mechanism of Schiff base formation and hydrolysis. J. Am. Chem. Soc. *84*, 832–837.

Chong, J.H., Sauer, M., Patrick, B.O., and MacLachlan, M.J. (2003). Highly stable keto-enamine salicylideneanilines. Org. Lett. *5*, 3823–3826.

Dey, K., Pal, M., Rout, K.C., H, S.K., Das, A., Mukherjee, R., Kharul, U.K., and Banerjee, R. (2017). Selective molecular separation by interfacially crystallized covalent organic framework thin films. J. Am. Chem. Soc. *139*, 13083–13091.

Enthaler, S., and Wu, X.-F. (2015). Zinc Catalysis: Applications in Organic Synthesis (Wiley-VCH Verlag GmbH & Co. KGaA).

El-Kaderi, H.M., Hunt, J.R., Mendoza-Cortés, J.L., Côté, A.P., Taylor, R.E., O'Keeffe, M., and Yaghi, O.M. (2007). Designed synthesis of 3d covalent organic frameworks. Science *316*, 268–272.

Fan, H., Gu, J., Meng, H., Knebel, A., and Caro, J. (2018). High-flux membranes based on the covalent organic framework COF-LZU1 for selective dye separation by nanofiltration. Angew. Chem. Int. Ed. *57*, 4083–4087.

Gao, S., Zhu, Y., Gong, Y., Wang, Z., Fang, W., and Jin, J. (2019). Ultrathin polyamide nanofiltration membrane fabricated on brush-painted single-walled carbon nanotube network support for ion sieving. ACS Nano *13*, 5278–5290.

Humphrey, W., Dalke, A., and Schulten, K. (1996). VMD: visual molecular dynamics. J. Mol. Graph. *14*, 33–38.

Jin, P., Zhu, J., Yuan, S., Zhang, G., Volodine, A., Tian, M., Wang, J., Luis, P., and Van der Bruggen, B. (2021). Erythritol-based polyester loose nanofiltration membrane with fast water transport for efficient dye/salt separation. Chem. Eng. J. *406*, 126796.

Karak, S., Kandambeth, S., Biswal, B.P., Sasmal, H.S., Kumar, S., Pachfule, P., and Banerjee, R. (2017). Constructing ultraporous covalent organic frameworks in seconds via an organic terracotta process. J. Am. Chem. Soc. *139*, 1856–1862.

Karan, S., Samitsu, S., Peng, X., Kurashima, K., and Ichinose, I. (2012). Ultrafast viscous permeation of

organic solvents through diamond-like carbon nanosheets. Science *335*, 444.

Karan, S., Jiang, Z., and Livingston, A.G. (2015). Sub-10 nm polyamide nanofilms with ultrafast solvent transport for molecular separation. Science *348*, 1347–1351.

Kandambeth, S., Biswal, B.P., Chaudhari, H.D., Rout, K.C., Kunjattu, H.S., Mitra, S., Karak, S., Das, A., Mukherjee, R., Kharul, U.K., and Banerjee, R. (2017). Selective molecular sieving in self-standing porous covalent-organic-framework membranes. Adv. Mater. *29*, 1603945.

Kandambeth, S., Mallick, A., Lukose, B., Mane, M.V., Heine, T., and Banerjee, R. (2012). Construction of crystalline 2d covalent organic frameworks with remarkable chemical (acid/base) stability via a combined reversible and irreversible route. J. Am. Chem. Soc. *134*, 19524–19527.

Liang, X., Wang, P., Wang, J., Zhang, Y., Wu, W., Van der Bruggen, b., and Liu, J. (2019). Zwitterionic functionalized MoS_2 nanosheets for a novel composite membrane with effective salt/dye separation performance. J. Membr. Sci. *573*, 270–279.

Li, Q., Liao, Z., Fang, X., Wang, D., Xie, J., Sun, X., Wang, L., and Li, J. (2019). Tannic acid-polyethyleneimine crosslinked loose nanofiltration membrane for dye/salt mixture separation. J. Membr. Sci. *584*, 324–332.

Martínez, L., Andrade, R., Birgin, E.G., and Martínez, J.M. (2009). PACKMOL: a package for building initial configurations for molecular dynamics simulations. J. Comput. Chem. *30*, 2157–2164.

Mayne, C.G., Saam, J., Schulten, K., Tajkhorshid, E., and Gumbart, J.C. (2013). Rapid parameterization of small molecules using the force field toolkit. J. Chem. Phys. *34*, 2757–2770.

Marchetti, P., Solomon, M.F.J., Szekely, G., and Livingston, A.G. (2014). Molecular separation with organic solvent nanofiltration: a critical review. Chem. Rev. *114*, 10735–10806.

Matsumoto, M., Valentino, L., Stiehl, G.M., Balch, H.B., Corcos, A.R., Wang, F., Ralph, D.C., Mariñas, B.J., and Dichtel, W.R. (2018). Lewis-acid-catalyzed interfacial polymerization of covalent organic framework films. Chem *4*, 308–317.

Matsumoto, M., Dasari, R.R., Ji, W., Feriante, C.H., Parker, T.C., Marder, S.R., and Dichtel, W.R. (2017). Rapid, low temperature formation of imine-linked covalent organic frameworks catalyzed by metal triflates. J. Am. Chem. Soc. *139*, 4999–5002.

Mobinikhaledi, A., Steel, P.J., and Polson, M. (2009). Rapid and efficient synthesis of Schiff bases catalyzed by copper nitrate. Synth. React. Inorg. Met. Org. Nano-metal Chem. *39*, 189–192.

Phillips, J.C., Hardy, D.J., Maia, J.D.C., Stone, J.E., Ribeiro, J.V., Bernardi, R.C., Buch, R., Fiorin, G., Hénin, J., Jiang, W., et al. (2020). Scalable molecular dynamics on CPU and GPU architectures with NAMD. J. Chem. Phys. *153*, 044130.

Sarkar, P., Modak, S., and Karan, S. (2020). Effect of porous and nonporous nanostructures on the permeance of positively charged nanofilm composite membranes. Adv. Mater. Inter. *7*, 2000251.

Sarkar, P., Ray, S., Sutariya, B., Chaudhari, J.C., and Karan, S. (2021a). Precise separation of small neutral solutes with mixed-diamine-based nanofiltration membranes and the impact of solvent activation. Separation Purif. Technol. *279*, 119692.

Sarkar, P., Modak, S., and Karan, S. (2021b). Ultraselective and highly permeable polyamide nanofilms for ionic and molecular nanofiltration. Adv. Funct. Mater. *31*, 2007054.

Sarkar, P., Modak, S., Ray, S., Adupa, V., Reddy, K.A., and Karan, S. (2021c). Fast water transport through sub-5 nm polyamide nanofilms: the new upper-bound of the permeance-selectivity trade-off in nanofiltration. J. Mater. Chem. A. *9*, 20714.

Schwab, M.G., Fassbender, B., Spiess, H.W., Thomas, A., Feng, X., and Müllen, K. (2009). Catalyst-free preparation of melamine-based microporous polymer networks through Schiff base chemistry. J. Am. Chem. Soc. *131*, 7216–7217.

Su, Y.-Y., Yan, X., Chen, Y., Guo, X.-J., Chen, X.-F., and Lang, W.-Z. (2021). Facile fabrication of COF-LZU1/PES composite membrane via interfacial polymerization on microfltration substrate for dye/salt separation. J. Membr. Sci. *618*, 118706–119204.

Tiwari, K., Sarkar, P., Modak, S., Singh, H., Pramanik, S.K., Karan, S., and Das, A. (2020). Large area self-assembled ultrathin polyimine nanofilms formed at the liquid-liquid interface used for molecular separation. Adv. Mater. *32*, 1905621.

You, X., Wu, H., Zhang, R., Su, Y., Cao, L., Yu, Q., Yuan, J., Xiao, K., He, M., and Jiang, Z. (2019). Metal-coordinated sub-10 nm membranes for water purification. Nat. Commun. *10*, 4160.

You, X., Xiao, K., Wu, H., Li, Y., Li, R., Yuan, J., Zhang, R., Zhang, Z., Liang, X., Shen, J., and Jiang, Z. (2021). Electrostatic-modulated interfacial polymerization toward ultra-permselective nanofiltration membranes. iScience *24*, 102369.

Yu, W., He, X., Vanommeslaeghe, K., and MacKerell, A.D., Jr. (2012). Extension of the CHARMM general force field to sulfonyl-containing compounds and its utility in biomolecular simulations. J. Comput. Chem. *33*, 2451–2468.

Yuan, D., Lu, W., Zhao, D., and Zhou, H.-C. (2011). Highly stable porous polymer networks with exceptionally high gas-uptake capacities. Adv. Mater. *23*, 3723–3725.

Yuan, S., Li, X., Zhu, J., Zhang, G., Van Puyvelde, P., and Van der Bruggen, B. (2019). Covalent organic frameworks for membrane separation. Chem. Soc. Rev. *48*, 2665–2681.

Vanommeslaeghe, K., Hatcher, E., Acharya, C., Kundu, S., Zhong, S., Shim, J., Darian, E., Guvench, O., Lopes, P., Vorobyov, I., and Mackerell, A.D., Jr. (2010). CHARMM general force field: a force field for drug-like molecules compatible with the CHARMM all-atom additive biological force fields. J. Comput. Chem. *31*, 671–690.

Vanommeslaeghe, K., and MacKerell, A.D., Jr. (2012a). Automation of the CHARMM general force field (CGenFF) i: bond perception and atom typing. J. Chem. Inf. Model. *52*, 3144–3154.

Vanommeslaeghe, K., Raman, E.P., and MacKerell, A.D., Jr. (2012b). Automation of the CHARMM general force field (CGenFF) ii: assignment of bonded parameters and partial atomic charges. J. Chem. Inf. Model. *52*, 3155–3168.

Wang, R., Shi, X., Xiao, A., Zhou, W., and Wang, Y. (2018). Interfacial polymerization of covalent organic frameworks (COFs) on polymeric substrates for molecular separations. J. Membr. Sci. *566*, 197–204.

Wei, T., Zhang, L., Zhao, H., Ma, H., Sajib, M., Jiang, H., and Murad, S. (2016). Aromatic polyamide reverse-osmosis membrane: an atomistic molecular dynamics simulation. J. Phy. Chem. B *120*, 10311–10318.

Zhang, Y., Ma, J., and Shao, L. (2020). Ultra-thin trinity coating enabled by competitive reactions for unparalleled molecular separation. J. Mater. Chem. A. *8*, 5078–5085.

Zhu, C., Liu, J., Li, M.-B., and Bäckvall, J.-E. (2020). Palladium-catalyzed oxidative dehydrogenative carbonylation reactions using carbon monoxide and mechanistic overviews. Chem. Soc. Rev. *49*, 341–353.

STAR★METHODS

KEY RESOURCES TABLE

REAGENT or RESOURCE	SOURCE	IDENTIFIER
Chemicals, solvents, salts, and dyes		
Phloroglucinol, 99.0%	TCI Chemicals (India)	CAS:108-73-6
Hexamethylenetetramine, 99.0%	TCI Chemicals (India)	CAS:100-97-0
Trifluoroacetic acid	TCI Chemicals (India)	CAS: 76-05-1
Methyl orange	TCI Chemicals (India)	CAS: 547-58-0
Orange G	TCI Chemicals (India)	CAS: 1936-15-8
Aniline blue	TCI Chemicals (India)	CAS: 6268-05-9
Brilliant blue R	TCI Chemicals (India)	CAS: 6104-59-2
Evans blue	TCI Chemicals (India)	CAS: 314-13-6
Rhodamine B	TCI Chemicals (India)	CAS: 81-88-9
NaCl (99.9%)	Sisco Research Laboratories Pvt. Ltd., India	CAS: 7647-14-5
Na_2SO_4 (99.5%)	Sisco Research Laboratories Pvt. Ltd., India	CAS: 7757-82-6
Melamine, 99.0%	Alfa Aesar chemicals	CAS: 108-78-1
Toluene, AR	MERCK Millipore, India	CAS: 108-88-3
Isopropanol, AR	MERCK Millipore, India	CAS: 67-63-0
Methanol, AR	MERCK Millipore, India	CAS: 67-56-1
Acetonitrile, AR	MERCK Millipore, India	CAS: 75-05-8
Dimethylformamide; 99% EMPLURA®	MERCK Millipore, India	CAS: 68-12-2
Polymer, membrane, and substrates		
Polyacrylonitrile (PAN) powder	IPCL, India	NA
Nonwoven polyester fabric	Nordlys-TS100, Polymer Group Inc., France	NA
N-type <100 > silicon wafer	University wafer, Boston, USA	https://universitywafer.com/
100 nm thick gold coated PLATYPUS™ silicon wafer	Agar Scientific, UK	https://www.agarscientific.com/
Porous alumina support; Whatman™ Anodisc™; 0.02 μm	Fisher Scientific	https://www.fishersci.com/
Software		
CasaXPS: Processing Software for XPS	Casa Software Ltd	http://www.casaxps.com/

RESOURCE AVAILABILITY

Lead contact

Further information and requests for resources and reagents should be directed to and will be fulfilled by the lead contact, Professor Santanu Karan (santanuk@csmcri.res.in).

Materials availability

This study did not generate new materials

Data and code availability

- Data: All data reported in this paper will be shared by the lead contact upon request.
- Code: This paper does not report the original code.

- Any additional information required to reanalyze the data reported in this paper is available from the lead contact upon request.

METHODS DETAILS

Experimental procedures

Synthesis of 2,4,6-triformylphloroglucinol (TFP)

2,4,6-triformylphloroglucinol (TFP) was synthesized according to the literature procedure (Chong et al., 2003). To a 100 mL round bottom flask containing phloroglucinol (1 g, 7.9 mmol) and hexamethylenetetramine (2.43 g, 17.38 mmol), 15 mL trifluoroacetic acid was added under N_2 atmosphere. The solution mixture was heated at 100°C for 2.5 h. To this, 9 mL of 3 M HCl was added, and then the solution was heated at 100°C for 1 h. After cooling to room temperature, the solution was filtered through celite, extracted with DCM, dried over Na_2SO_4, and filtered. DCM was removed under reduced pressure, and finally, the obtained compound was purified by washing with methanol for 2–3 times. The molecular structure of TFP was confirmed by IR and NMR spectroscopy.

Color: off-white solid; Yield 0.229 g (13.9%); ^{1}H NMR (δ ppm $CDCl_3$): 14.10 (s, 3H, -OH), 10.11 (s, 3H, -CHO); ^{13}C NMR (δ ppm $CDCl_3$): 192.14 (CHO), 173.36 (COH), 102.95 (CCHO). IR (KBr): ν (cm^{-1}) = 3425, 2920–2845, 1637.

Preparation of the organic phase solution for interfacial polymerization

TFP has limited solubility in non-polar organic solvents (toluene or hexane). Therefore, to enhance solubility in the said solvents, TFP (0.023 wt%) was suspended in a highly polar solvent, DMSO (0.13 wt%) under sonication for 1 min. Moreover, acetic acid (0.061 wt%) was added in the DMSO suspended TFP, which enhances TFP solubility in DMSO by protonation of TFP and acts as a catalyst for interfacial polymerization reaction (Figure S3). Further, to this solution mixture toluene (99.81 wt%) was added and stirred for 2 h at 70°C.

Preparation of the aqueous phase solution for interfacial polymerization

The aqueous solution was prepared with 0.1 wt% melamine and 0.02 wt% $Cu(ClO_4)_2.6H_2O$ and stirred at room temperature.

Preparation of polyimine nanofilm composite membranes

The polyimine nanofilm composite membranes were prepared on HPAN support membranes via interfacial polymerization. The room temperature and the relative humidity were maintained at 22 ($\pm$1) °C and 50 ($\pm$5)%, respectively. Firstly, HPAN support membranes of size 15 × 30 cm were washed with pure water to remove excess isopropanol, where they were stored. The aqueous phase solution was poured on top of a rectangular HPAN support and soaked for 30 s. After discarding the aqueous solution, the excess water that remained on the support surface was removed with a rubber roller followed by air-drying for 20 s. The organic phase solution was then poured on the melamine-soaked support and left for a designated time of 15 s or 2 min to undergo polymerization reaction and the formation of polyimine nanofilm composite membrane. The organic solution was discarded and dried at room temperature for 20 s and finally annealed at a temperature of 70 ($\pm$1) °C for 3 min in a hot air oven. Polyimine nanofilm composite membranes prepared for a reaction time of 15 s were further post-treated with dimethylacetamide (DMAc), methanol, an aqueous solution of NaOH (pH = 7.4 to 10). In another experiment, to know the effect of the room environment, the room humidity was maintained at 87 ($\pm$5)%. Membrane preparation conditions are provided in Table S1.

Preparation of freestanding polyimine nanofilms

Freestanding polyimine nanofilms were prepared at organic (toluene-DMSO) and aqueous phase interface via the interfacial polymerization of TFP and melamine in the presence of CH_3COOH added in the organic phase and $Cu(ClO_4)_2.6H_2O$ added in the aqueous phase. In a typical example, 0.023 wt% of TFP and 0.061 wt% of acetic acid were taken in toluene (99.81 wt%)-DMSO (0.13 wt%) solution. Toluene-DMSO solution was poured carefully on the top surface of the aqueous phase containing melamine (0.1 wt%) and $Cu(ClO_4)_2.6H_2O$ (0.02 wt%) and left undisturbed for a designed time. The freestanding polyimine nanofilms were transferred onto the different supports (silicon wafer, gold-coated silicon wafer, TEM copper grid, porous anodic alumina, etc.) for SEM, TEM, AFM, and XPS analysis.

Preparation of ultrafiltration polyacrylonitrile (PAN) and hydrolyzed PAN (HPAN) support membranes

Ultrafiltration PAN support membranes were prepared on a nonwoven fabric using a continuous casting machine following the phase inversion technique (Sarkar et al., 2021b). PAN polymer powder was dried in a hot air oven at 70 (±1) °C for 2 h before dissolving in DMF (13 w/w%) under the stirring condition at 70 (±1)°C in an air-tight glass bottle. The polymer solution was then cooled to room temperature and left overnight for degassing. A roll-to-roll semi-automated continuous casting machine with a knife gap set at 150 μm was used to cast the dope solution on the smooth side of the nonwoven fabric at a temperature of 25 (±1)°C for the preparation of ultrafiltration membranes via phase inversion in water. The membrane roll was cut into small pieces, and the excess DMF was removed by keeping the membrane pieces in freshwater for two days and finally stored at 10 (±1)°C in isopropanol and water (1:1 v/v) mixture.

HPAN support membranes were prepared by the hydrolysis of PAN ultrafiltration supports, as discussed in our earlier publication (Sarkar et al., 2021b). Several pieces (~75 nos.) of PAN supports were washed thoroughly in pure water and then immersed in a 5 L of 1 M sodium hydroxide (NaOH) solution preheated in a hot air oven at 60 (±1) °C for 2 h and the solution was again placed in the hot air oven at 60 (±1) °C for 2 h to allow hydrolysis. Hydrolyzed membranes were transferred in pure water and washed for a few days by periodically exchanging the water with fresh water. Finally, the HPAN membranes were stored at 10 (±1) °C in isopropanol and water mixture (1:1 v/v).

Performance evaluation of the polyimine nanofilm composite membranes

The nanofiltration performance of the composite membranes was tested at 25 (±1)°C in a cross-flow filtration setup (Sarkar et al., 2021b) with a cross-flow velocity of 35–40 L h^{-1}. Feed solution (≈10 L) was pumped from a feed tank using a high-pressure diaphragm pump into the membrane cell. The effective area of the membranes used in the cell was 14.5 cm^2. Membranes were pre-compacted for at least 8 h under 2 bar or 5 bar (as mentioned in the main text) using pure water to achieve the steady-state conditions. Membrane permeances were calculated by using the following equation:

$$P = \frac{V}{A.t.\,\Delta p}$$

where V is the volume of the permeate in liters, t (h) is the collection time, A (m^2) is the effective area of the membrane, and Δp (bar) is the transmembrane pressure.

The separation performance of the polyimine composite membranes was analyzed by using different salts and dyes added in the aqueous feed. For a single solute feed, the concentration of NaCl and Na_2SO_4 was 2 g $L^{-1,}$ and the concentration of methyl orange (MO), Orange G (OG), aniline blue (AB), brilliant blue R (BBR), Evans blue (EB) and rhodamine B (RhB) was 0.2 g L^{-1}. For the mixed feed of salt and dye, the salt concentration was 2 g L^{-1}, and the dye concentration was 0.2 g L^{-1}. For the mixed feed of a combination of dyes, the concentration of each dye was 0.1 g L^{-1} with a total concentration of 0.2 g L^{-1}. The concentration of salts and dyes in the permeate and feed was evaluated by an electrical conductivity meter and the UV-visible absorption spectrophotometer, respectively. Absorption spectra were recorded after necessary dilution. The rejection (R%) of the solutes was calculated according to the following equation:

$$R(\%) = \left(1 - \frac{C_p}{C_f}\right) \times 100$$

where C_p (in g L^{-1}) and C_f (in g L^{-1}) are the concentrations of solutes in the permeate and the feed, respectively. To get an average value and the standard deviation, at least four membrane coupons were tested.

Molecular dynamics simulations

Molecular dynamics simulations were performed to calculate the pore size distribution and other properties of the membrane at the molecular level. The membrane was constructed in a heuristic manner where a distance criterion is employed to form an imine bond between the monomers, triformylphloroglucinol (TFP) and melamine. This distance was relaxed as the polymerization goes further to increase the rate of formation of imine bonds between the monomers. Initially, monomers were packed in a simulation box using PACKMOL (Martínez et al., 2009). Minimization was done for 10000 steps, and the system was allowed to equilibrate for 2 ns in NPT ensemble at a temperature of 300 K and 1 atm pressure. Then the system was subjected to an annealing process in an NVT ensemble, where the temperature was raised to 1100 K and

cooled back to 300 K with a step size of 50 K. The simulation was continued by allowing new imine bonds formation for every 10 ps of simulation time. The bond formation was allowed only when the distance between C1/C2/C3 of TFP and N1/N2/N3 of melamine (Figure S5) was less than 2.5 Å, and as the simulation progressed, this was relaxed to 3.5 Å with a step of 0.1 Å to speed up the crosslinking process. In the end, unreacted monomers were removed from the membrane and the structure was used as the initial configuration for the next step.

All the force field parameters for monomers and the polymer were obtained from CHARMM General Force Field (CGenFF) (Vanommeslaeghe et al., 2010, 2012b; Yu et al., 2012; Vanommeslaeghe and MacKerell, 2012a) interface version 1.0.0 and the force field version 3.0.1. All the simulations were carried out on NAMD (Philips et al., 2020). We observed penalties in dihedral parameters, which were re-optimized using fftk, an automated force field parameterization toolkit (Mayne et al., 2013) widely distributed as a plugin to the molecular visualization software VMD (Humphrey et al., 1996). Parameters were obtained based on QM-determined potential energy surfaces (PES), generated by scanning dihedrals of interest (with penalty) at MP2/6-31G(d) level of theory. Dihedrals scan calculations were done using Gaussian 16 (Mayne et al., 2013). The resulting QM-PES was fitted to a molecular mechanics (MM) potential energy surface using fftk. The initial optimization shows a poor fit to the QM data. Further refinement of the dihedral parameters was performed by altering the multiplicity and periodicity settings to get the shape of MM PES to match QM data (Figures S6 and S7). The optimized dihedral parameters were used for the simulations.

Equilibrium molecular dynamics simulations

The membrane obtained after polymerization was solvated in water using a solvate plugin in VMD. The resulting membrane was 150 Å thick and 130 Å in X and Y directions. Equilibration was performed on this solvated system for 3 ns in an NPT ensemble at 300 K and 1 atm pressure. All the analysis was done for the last 1 ns of the simulation trajectory. Density profiles of water, membrane, and the overall system were calculated (Figure 1G, main text). For the last 1 ns, we have calculated the pore size distribution (PSD) of the membrane for every 100 ps and averaged. PSD calculations were done with a test particle radius of 1.0 Å and found prominent pores with a radius of 4.5 Å to 6 Å (Figure 1F, main text).

Characterization techniques

Fourier transformed infrared spectra (FTIR) was recorded in a KBr pellet on a Perkin Elmer FT-IR spectrophotometer in 4000–400 cm^{-1} region in the transmission mode. Polyimine nanofilm as a powder was made via interfacial polymerization at the bulk organic-aqueous interface in the presence of $Cu(ClO_4)_2$. Nanofilms were collected from the interface, repeatedly washed in water and methanol, and dried. The interfacial polymerization conditions were kept identical to the freestanding nanofilm (see the main text).

X-ray photoelectron spectroscopy (XPS) study was conducted on freestanding polyimine nanofilms. Nanofilms were made at the bulk organic-aqueous interface in the presence of $Cu(ClO_4)_2$, and transferred onto a PLATYPUS™ gold-coated silicon wafer. The gold-coated silicon wafer containing nanofilm was then dried at room temperature, washed in methanol by immersing in methanol for 15 min, and finally dried in a hot air oven at 50°C for 15 min. The X-ray photoelectron spectroscopy (XPS) study was carried out using Thermo Scientific ESCALAB 250 Xi XPS using monochromatic AlKα X-ray as an excitation source outfitted with an X-ray spot size of 650 × 650 μm^2. The survey spectra and core-level XPS spectra were recorded from at least three different spots on the samples. The analyzer was operated at pass energy of 150 eV for survey scans and 20 eV for narrow scans with the C1s SP3 hydrocarbon peak set at BE 284.8 eV. A low-energy electron flood gun was used to overcome sample charging. Data processing was performed using Thermo Scientific™ Avantage data system and CasaXps processing software. Peak areas were measured after satellite subtraction and background subtraction, either with a linear background or following the methods of Shirley. The deconvolution of the core-level spectra was done by choosing a Shirley or spline Tougaard background with GL(30) line shape (70% Gaussian, 30% Lorentzian) to determine the chemical species of the nanofilm.

Scanning electron microscopy (SEM) images were obtained from a high-resolution scanning electron microscope (SEM; JEOL JSM 7100F, Japan) with an accelerating voltage of 15 kV. Samples were prepared on silicon wafer substrate/HPAN support/alumina support, and ≈4 nm thin gold coating was sputtered deposited (EM ACE200, Leica Microsystems) to avoid sample charging under the electron beam.

A transmission electronic microscope (TEM; JEOL JEM 2100, Japan) operated at 200 kV was used to study the surface morphology of the freestanding polyimine nanofilms transferred onto copper grids.

Atomic Force Microscope (AFM; NT-MDT Spectrum Instruments, NTEGRA Aura) with a pizzo type scanner was used to measure surface morphology and thickness of the polyimine nanofilms. Sampling resolution was 256 or 512 points per line with a speed of 0.5–1.0 Hz. High resolution noncontact "golden" silicon AFM cantilevers NSG10 series was obtained from NT-MDT Spectrum Instruments, Moscow, Russia. The length, width, and thickness of the cantilever were 95 μm, 30 μm, and 2 μm, respectively. The typical resonant frequency and force constant were 240 kHz and 11.8 N/m, respectively. Freestanding polyimine nanofilms were made at the bulk organic-aqueous interface and transferred onto a silicon wafer. For thickness measurement, a scratch was made to expose the silicon wafer, and the height difference was recorded from AFM. Gwyddion 2.50 SPM software was used for AFM image analysis.

Zeta Cad streaming current & zeta potential meter was used to measure the surface charge of polyimine composite membranes. Two pieces of membranes with a dimension of 3 × 5 cm^2 were cut and kept in the KCl solution overnight before use. Zeta potential values were obtained at pH 7 using a 0.1 M KCl solution.

UV-visible absorption spectra of the feed and permeate were recorded by Shimadzu UV-2600 spectrophotometer in the range of 200–800 nm. The solutions were diluted in the water where necessary.

QUANTIFICATION AND STATISTICAL ANALYSIS

We report the average values of water permeance, salt, and molecular rejections, and standard deviations of the results based on the measurements of at least four sets of membrane coupons.